Pressure-induced polyamorphism in a main-group metallic glass

Min Wu,[1,2,3,4] Hongbo Lou,[2] John S. Tse,[3,5,*] Hanyu Liu,[5] Yuanming Pan,[4] Kazushi Takahama,[6] Takahiro Matsuoka,[6] Katsuya Shimizu,[6] and Jianzhong Jiang[2,†]

[1]*College of Materials Science and Engineering, Zhejiang University of Technology, Hangzhou 310014, People's Republic of China*

[2]*International Center for New-Structured Materials, State Key Laboratory of Silicon Materials, and School of Materials Science and Engineering, Zhejiang University, Hangzhou 310027, People's Republic of China*

[3]*Department of Physics and Engineering Physics, University of Saskatchewan, Saskatoon, Saskatchewan, Canada S7N 5E2*

[4]*Department of Geological Sciences, University of Saskatchewan, Saskatoon, Saskatchewan, Canada S7N 5E2*

[5]*State Key Laboratory of Superhard Materials, Jilin University, Changchun 130012, People's Republic of China*

[6]*KYOKUGEN, Graduate School of Engineering Science, Osaka University, Osaka 560-8531, Japan*

(Received 28 August 2015; published 25 August 2016)

The mechanism of pressure-induced amorphous-to-amorphous transitions (AATs) in metallic glasses (MGs) has been a subject of intense research. Most AATs in MGs were found in lanthanide-based alloys and shown to originate from $4f$ orbital delocalization. Recently, evidence of an unexpected AAT in the main-group Ca-Al MGs was reported without a satisfactory explanation. Here, based on the results of first-principles molecular dynamics calculations, the suggested AAT at 12–15 GPa in the $Ca_{72.7}Al_{27.3}$ MG is confirmed. Contrary to the common belief that the coordinate of metallic glasses with close packing cannot be increased further, the coordination around Al atoms is found to increase suddenly at the transition as a consequence of atomic migration and the aggregation of Al atoms. This transition originates from pressure-enhanced bonding between Ca $3d$ and Al $3p$ orbitals and is confirmed by the good agreement on the predicted and measured electrical conductivities. The theoretical analysis not only uncovers a mechanism of pressure-induced AAT in main-group MGs, but it can be generalized to establish a different perspective to guide the understanding of transformation phenomena in compressed MGs.

DOI: 10.1103/PhysRevB.94.054201

I. INTRODUCTION

Pressure is a versatile and controllable thermodynamic variable that can significantly modify the interactions between atoms that often lead to a variety of critical phenomena [1–4]. Pressure-induced amorphous-amorphous transitions (AATs) in metallic glasses (MGs) are one of the most challenging and outstanding problems. Polyamorphism in nonmetallic amorphous systems has been studied extensively, e.g., in amorphous ice [5], oxides [6], chalcogenides [7], and silicon [8]. In these systems, atoms or groups of atoms are connected by directional covalent or ion-covalent bonds, and pressure-induced AATs are related to the densification of the network structure and the increase of the atom local coordination. However, the structure of MGs obtained by a rapid quench from the melts is generally believed to be similar to a liquid that has already achieved a random close-packed structure. Therefore, polyamorphism in MGs thus raises a fundamental question: "How can a structure that has already achieved close packing be compressed to an even denser form?" [9–13]. Pressure-induced AATs are often found in lanthanide-based MGs [10,11,14,15], and the structural transitions are attributed to $4f \rightarrow 5d$ orbital hybridization of the lanthanide atoms, where electrons are transferred from a spatially localized $4f$ orbital to the itinerant $5d$ orbital, a suggestion supported by x-ray absorption spectroscopic measurements [10]. It is suggested that the reduced size of the lanthanide atoms leads to a low- to high-density polyamorphic transition. Therefore, it is surprising that evidence of an AAT was recently reported in main-group Ca-Al MGs without $4f$ orbitals [12]. Previously, following the known high-pressure behavior of crystalline pure Ca, it was suggested that this polyamorphic transition may be caused by a Ca $4s \rightarrow 3d$ electron transfer [12]. No direct experimental evidence or theoretical verification was offered to support this conjecture. The suggestion, however, contradicts an earlier electronic structure calculation showing that the Ca $3d$ orbitals are already actively involved in the bonding of Ca-Al alloys at ambient pressure [16]. From a recent successful study on the revitrification (recrystallization) of a $Ce_{75}Al_{25}$ MG [17], we demonstrated that the difference in the volume compression of the two atoms in a binary system is an important factor affecting the AAT in Ca-Al glasses. To test this hypothesis, first-principles molecular dynamics (FPMD) calculations were performed on an a-$Ca_{72.7}Al_{27.3}$ MG. Although FPMD calculations suffer from a limited time scale compared to experiment, they are able to describe the short-range order structure of disordered systems quite well and have been used extensively in metallic glass simulations. As will be described in detail below, the observed AAT transition at ~15 GPa [12] was confirmed. The calculations reveal a discontinuity in the charge back-donation from Al to Ca at the structural transition due to enhanced overlaps between the Al $3p$ orbitals with $3d$ orbitals of the positively charged Ca and concomitantly increasing the local coordination around the Al. The orbital rehybridization is confirmed by *in situ* measurements of the electrical resistance of a-$Ca_{72.7}Al_{27.3}$ with the four-probe method [18] (see the Supplemental Material for details of theoretical and experimental methods [19]). This interpretation refutes the proposed mechanism based on the analogy with the $4f$ orbital delocalization in

*john.tse@usask.ca
†jiangjz@zju.edu.cn

lanthanide-based MGs. Drawing from knowledge gained from recent studies of pressure-induced revitrification in Ce-Al MG and disordered SnI_4 [17,20], we recognized the importance of a nonuniform reduction of the atom sizes and, therefore, the relative ratios, due to a continuous change of electronic structure in multicomponent glasses. An unexpected result is the aggregation of Al in the metallic glass. This may provide an alternate route to the formation of a nanoglass which possesses very distinctive properties from the bulk [21]. The results presented here offer a perspective to interpret pressure-induced structural transformation phenomena in MG and possible different directions in the fabrication of nanostructures in glass.

II. RESULTS AND DISCUSSION

A. Equation of state and structural analysis

The pressure-volume curve [equation of state (EOS)] of a model a-$Ca_{72.7}Al_{27.3}$ consisting of 176 atoms is shown in Fig. 1(a). It shows a discontinuity at 12–15 GPa, which indicates the transformation from a low-density to high-density

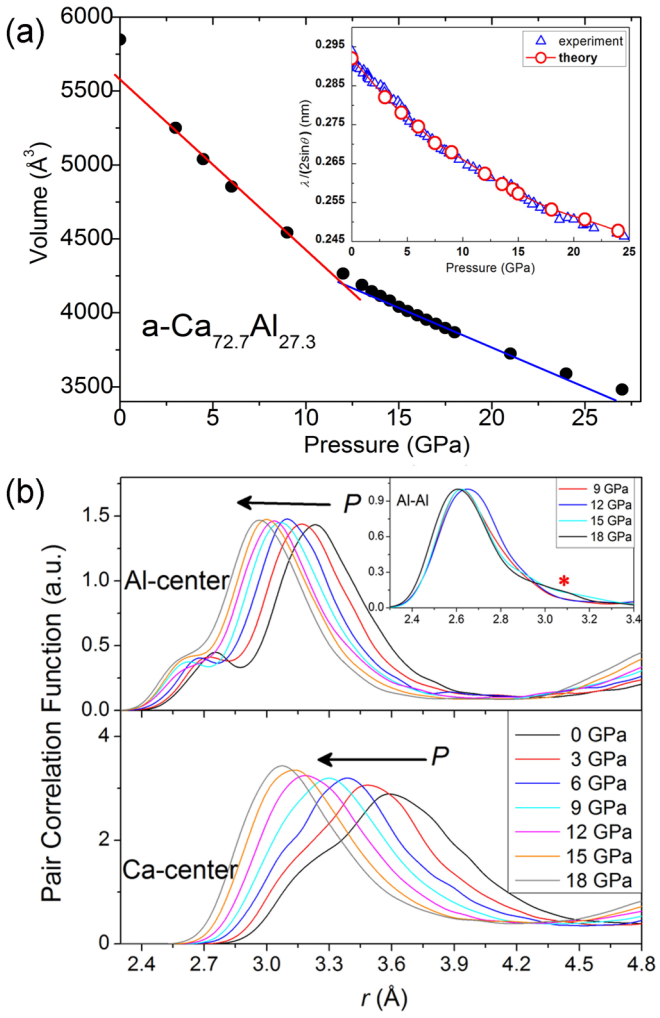

FIG. 1. (a) Equation of states of a-$Ca_{72.7}Al_{27.3}$. The inset shows the comparison of $\lambda/(2\sin\theta)$ between experiment and theoretical results. (b) Partial PCFs of a-$Ca_{72.7}Al_{27.3}$ under pressure. The inset shows Al-Al partial PCFs at selected pressures. The red star shows the development of a broad shoulder at ~3.1 Å between 15 and 18 GPa.

form. The predicted positions of the first sharp diffraction peak [FSDP, $\lambda/(2\sin\theta)$] are compared with the experiment results [inset of Fig. 1(a)] and good agreements are found. The high-density amorphous structure after the AAT has a smaller compressibility compared to that before the transition. Atomic pair correlation functions (PCFs) of a-$Ca_{72.7}Al_{27.3}$ calculated at different pressures are shown in Fig. 1(b). At ambient pressure, two peaks at 3.25 and 3.60 Å are found in the partial Ca-centered PCF, corresponding to the nearest-neighbor Ca-Al and Ca-Ca, respectively. In the partial Al-centered PCF, the small peak at 2.75 Å is attributed to the closest Al-Al pairs. In comparison with the Al-Al distance of 2.86 Å for face-centered-cubic Al, a shorter Al-Al separation in the alloy indicates that Al aggregates are formed in the amorphous structure from cooling of the melt. This is also confirmed by a visual inspection of the structure. It is intriguing that Al aggregates have also been found by experiments in Ce-Al and La-Al MGs [22,23]. It appears that under nonequilibrium conditions, the formation of Al aggregates maybe a general feature in Al-containing MGs. At high pressure, the Ca-Al and Ca-Ca peaks are merged and the distributions become narrower. The result indicates that the difference between Ca-Al and Ca-Ca interatomic distances becomes very small at high pressure and the local packing around the Ca atoms is more uniform. More significantly, as shown in the inset of Fig. 1(b), a sudden change in the Al-Al PCF profile between 12 and 15 GPa is observed. Unexpectedly, the position of the first peak shifts from 2.61 Å at 9 GPa to 2.66 Å at 12 GPa. When further compressed to 15 GPa, the peak shifts back to 2.61 Å with a distinctive shoulder at 3.1 Å. The initial decrease in the nearest Al-Al separation is understood by a compression effect. When the pressure increases further, the Al atoms in the second atomic shell are pressed closer to the central Al atom which leads to an increase of the local Al coordination. When the nearest-neighbor Al atoms become too crowded to alleviate the unfavorable repulsive interaction, the interatomic distance is increased.

Most reports on AATs in lanthanide-based MGs were ascribed to pressure-induced $4f$ electron delocalization as a result of orbital rehybridization [10,11,14,15] (*vide supra*). However, the Al-Al partial PCF clearly shows that a change of the local atomic packing also affects the coordination number (CN). To further investigate this possible linkage, a thorough analysis of the CN has been performed. The CN is obtained from the integration of the PCF from the origin of the atom to a prescribed cutoff radius, which is chosen as the distance at the first valley in the PCFs. For example, the CN of Al_C-Ca shown in Fig. 2(a) is the average number of Ca atoms surrounding the Al_C atom, where the subscript "C" denotes the "central atom." An increase of the total CN of the Al atom from 10.1 at ambient pressure to 11.5 at 21 GPa is found. The total CN of the Ca atom, however, remains almost constant at ~13.8 with pressure. Although the total average CN of the Ca atom apparently remains constant, the chemical environment around the atom is changed with pressure. Specifically, the partial CN of Ca_C-Ca decreases from 10.2 at ambient pressure to 9.9 at 21 GPa. This decrease, however, is accompanied by a concomitant increase in the partial CN of Ca_C-Al from 3.6 to 3.9 in the same pressure range, including a sudden jump near 9–12 GPa. The change in the nature of the surrounding atoms is demonstrated

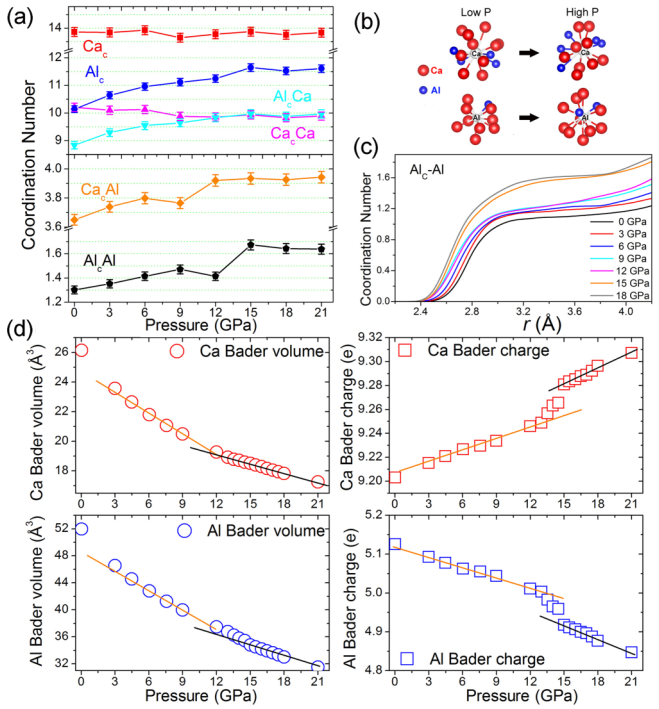

FIG. 2. Coordination number and Bader analysis. (a) Total and partial coordination number of a-$Ca_{72.7}Al_{27.3}$ under pressure. The subscript "C" represents the central atom. (b) Selected Ca- and Al-centered cluster before and after the AAT. The white spheres are the central atoms labeled separately. Note the intrusion of a second Al into the first coordination sphere of Al after AAT. (c) Cutoff radius-dependent integrated coordination number of Al_C-Al at different pressures. (d) Bader atomic volume and charge of a-$Ca_{72.7}Al_{27.3}$.

in Fig. 2(b) from the analysis of a selected cluster with a central Ca atom. For the central Al atoms, the number of the nearest-neighbor Ca increases from 8.8 at ambient pressure to 9.9 at 21 GPa. Above 12 GPa, the values of CN (Ca_C-Ca) and CN (Al_C-Ca) are close to each other. This observation is consistent with the similar interatomic Ca-Ca and Al-Ca distances at high pressures, discussed in the analysis of the PCF (*vide supra*). An increase in the CN of Al_C-Al at 12–15 GPa is also reflected in the Al-Al PCF shown in Fig. 1(b). This is illustrated in a selected cluster with a central Al atom shown in Fig. 2(b). To avoid bias introduced by the arbitrariness in the cutoff radius, a "running" CN of Al_C-Al is presented in Fig. 2(c). A discontinued increase in the CN of Al_C-Al indeed occurred.

B. Bader atomic analysis

The Bader quantum theory of atom-in-molecule is an unbiased way to characterize changes in "atomic" charges and volumes in a glass and have shown to play a key role in the amorphous-to-crystalline structural transition in Ce-Al MGs [17]. Here we applied the same analysis to a-$Ca_{72.7}Al_{27.3}$. The results are summarized in Fig. 2(d). A discontinuity in the charge is found close to the experimental AAT at ∼12 GPa [12]. The electronic structure calculation on a-$Ca_{72.7}Al_{27.3}$ at ambient pressure shows that the Ca-Al

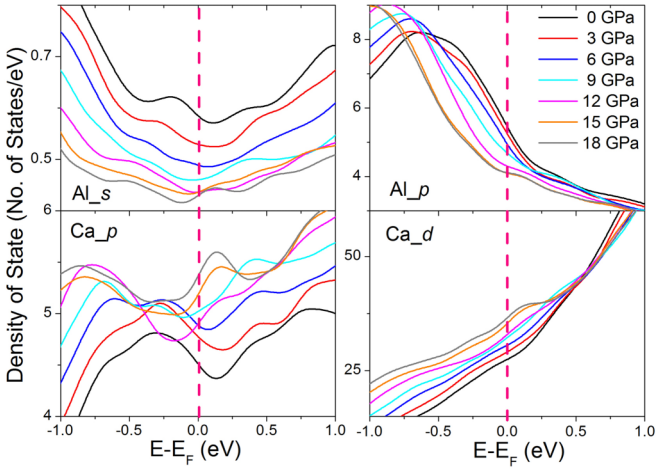

FIG. 3. PDOS of a-$Ca_{72.7}Al_{27.3}$ at different pressures. The Fermi level is set to 0.0 eV.

interaction is highly ionic even though a-$Ca_{72.7}Al_{27.3}$ is a metal. Due to the large electronegativity difference between Ca and Al, each Al atom gains ∼2.13e from the Ca atom. The calculated Bader atomic volume reflects this effect with the volume of the Al atom (51.97 $Å^3$) being about two times as large as the Ca atom (26.14 $Å^3$). With increasing pressure, the Bader charge shows that the Al atoms back-donate electrons gradually to the Ca atoms. At 12–15 GPa where the AAT is predicted in the EOS plot (*vide supra*), there are clear discontinuities in both the Bader atomic charges and volumes of Ca and Al as well. From the pressure dependency of the Ca and Al atoms, both atoms have a smaller compressibility after the AAT, which is consistent with the EOS shown earlier [Fig. 1(a)]. Between 12 and 15 GPa (i.e., at the AAT), an increase in the charge back-donation from Al to Ca is found. At this pressure range, the Bader charges show an average electron transfer of 0.1e from Al to Ca. In a-$Ca_{72.7}Al_{27.3}$, the Bader volume of the Al atom is always larger than that of the Ca atom within the pressure range studied (0–21 GPa). After the AAT, the Bader volume of the Al atom decreases faster with increasing pressure than that of Ca. The V_{Al}/V_{Ca} ratio remains fairly large and neither the Al nor Ca atoms can dominate the packing, therefore, no amorphous-to-crystalline transition is observed within the pressure range studied.

C. Density of States and electrical resistivities

To investigate the electronic factor contributing to the polyamorphic transition, the electronic density of states of a-$Ca_{72.7}Al_{27.3}$ have been calculated and are shown in Fig. 3. The projected DOS (PDOS) of a-$Ca_{72.7}Al_{27.3}$ show, unlike elemental Ca, that the Ca 3d orbitals dominate the valence band already at ambient pressure. With increasing pressure, the Al atoms donate electrons back to Ca (Al s-PDOS, Fig. 3). Remarkably, the profiles of the PDOS for both Ca and Al changed near 12 GPa. At lower pressure, both Ca and Al PDOS show a free-electron-like behavior. A "hump" starts to appear in all PDOS at about 12 GPa. The similarities in the PDOS profiles between Ca 3p,3d and Al 3p orbitals indicate there are

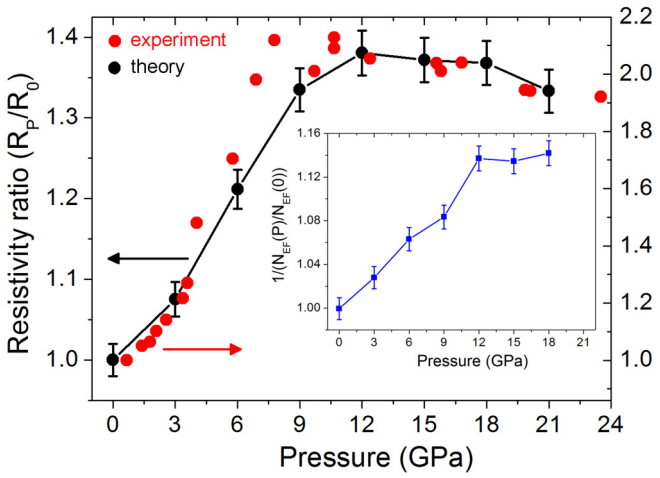

FIG. 4. Pressure-dependent relative electrical resistivity of a-$Ca_{72.7}Al_{27.3}$. The red and black circles represent experimental data and theoretical results, respectively. The inset shows the relative reciprocal number of states at the Fermi level as a function of pressure.

significant interactions between the atoms above 12 GPa. This is a consequence of a shorter Ca-Al distance at high pressure, which enhances the orbital overlaps and facilitates the charge back-donation (*vide supra*).

As discussed above, the electronic structure is modified at the AAT with an increase of covalent interactions (orbital overlaps) in the dense structure. We expect these changes will manifest in the electron transport property, in particular, the electrical resistivity (conductivity). To verify the theoretical prediction, we have calculated the electrical resistivity as a function of pressure. The resistivity was calculated from the Kubo-Greenwood formula by averaging 20 uncorrelated instantaneous structures of the glass taken from the trajectories of FPMD calculations. Within the framework of the Kubo-Greenwood independent particle approximation, the electrical conductivity as a function of frequency ω is

$$\sigma_1(\omega) = \frac{2\pi}{3\omega\Omega}\sum_k \omega(k)\sum_{j=1}^{N}\sum_{i=1}^{N}\sum_{\alpha=1}^{3}[f(\varepsilon_i,k) - f(\varepsilon_j,k)] \times |\langle\Psi_{j,k}|\nabla_\alpha|\Psi_{i,k}\rangle|^2\delta(\varepsilon_{j,k} - \varepsilon_{i,k} - \hbar\omega),$$

where ω is the frequency, Ω is the volume of the supercell, N is the total number of energy bands used, $\Psi_{i,k}$ and $\varepsilon_{i,k}$ are the electronic eigenstates and eigenvalues for the electronic state i at k, $f(\varepsilon_{i,k})$ is the Fermi distribution function, and $\omega(k)$ represents the k-point weighing factor. The dc conductivity σ_{dc} is then calculated from the frequency dependence $\sigma(\omega)$ in the limit at which $\omega \to 0$ [24]. A comparison of the calculated resistivities and experimental resistances measured by the four-probe method in a diamond anvil cell relative to the respective zero-pressure values is shown in Fig. 4. The predicted pressure trend of the resistivity is in agreement with the measurements, although the calculated relative resistivities (R/R_0) are slightly smaller than the experimental values. The calculated resistivity curve (Fig. 4) increases with pressure up to ~12 GPa and then decreases very slightly. A similar reversal of the resistance is found at ~10 GPa in the experiments. Moreover, both theory and experiment exhibit a plateau region and then decrease gradually after the AAT. To investigate the correlation the resistivity and orbital hybridization described above, the reciprocal of the number of electronic states at the Fermi level $[1/N(E_f)]$ is plotted as a function of pressure in the inset of Fig. 4. The plot shows a similar pressure trend as the predicted resistivity. From the analysis of the theoretical electronic density of states as presented above, we found that the initial rise in the resistivity can be explained as follows: At ambient pressure, a significant charge transfer from Ca to Al occurs due to the large electronegativity difference. As the pressure increases, charge back-donates from Al to the more localized Ca $3d$ orbitals, concomitantly the total density of states at the Fermi level decreases, and the electrical resistivity increases (the electrical conductivity decreases). After the AAT, and as a result of Ca $3d$ and Al $3p$ orbital mixing (overlaps), the system becoming more covalent and the number of electronic states at the Fermi level does not vary noticeably with a further increase of pressure. Consequently, the electrical resistance is not seriously affected by pressure, as observed in Fig. 4. The qualitative agreement between the theoretical predictions and experimental measurements confirms the theoretical findings and validates the mechanism of AAT presented above in a-$Ca_{72.7}Al_{27.3}$.

III. CONCLUSIONS

In conclusion, FPMD calculations were used to characterize the pressure effect of a main-group a-$Ca_{72.7}Al_{27.3}$MG. Upon compression, in agreement with experiments [12], an AAT is found at 12–15 GPa. Contrary to lanthanide-based MGs in which the pressure-induced AATs were driven by $4f \to 5d$ electron delocalization [10,11,14,15], the pressure-induced AAT in a-$Ca_{72.7}Al_{27.3}$ is caused by the enhancement of covalent interactions between Ca $3d$ and Al $3p$ electrons. This origin, revealed from Bader analysis, shows that the electron back-donation from the Al atoms to the Ca atoms suddenly increases between 12 and 15 GPa. The enhanced overlaps between Ca $3d$ and Al $3p$ orbitals at the polyamorphic transition promote interactions between Ca and Al and modify the local atomic packing. Furthermore, the interactions between Al atoms in the aggregates result in the increase of the Al local (Al_C-Al) CN. As a result, charge sharing between Al atoms increases, which favors more electron back-donation to the Ca atoms. The electronic changes affect the local atomic packing and the amorphous structure transforms from a low-density to a high-density form. This conclusion is further supported by the agreement between predicted and measured pressure-dependent resistivities and resistances, respectively. Initially, the resistivity is found to increase with pressure, due to an increased Ca $3d$ occupation from the electron back-donation from Al and a decreased total density of states at the Fermi level. This trend is reversed after the polyamorphic transition and the resistivity remains relatively constant with increasing pressure. The slight decrease in the resistivity is consistent with a slight increase in the density of states at the Fermi level, which is a result of the mixing of Ca $3d$ and Al $3p$ orbitals. The present results are in sharp contrast to the f-electron-containing MGs. The observation of an increase in the coordination number of the Al atom accompanying

the AAT in the a-$Ca_{72.7}Al_{27.3}$ alloy challenges the common view that the coordination number in close-packed MGs could not be easily increased by compression. The AAT in a-$Ca_{72.7}Al_{27.3}$ is due to an enhanced orbital overlap during compression. The information provided here might change conventional thinking about the structure of MGs, particularly under pressure. In a binary metallic glass when the structure has already achieved close packing and if both atoms contract uniformly with compression, i.e., the volume ratio remains constant, a structural transition is not possible. A structural change occurs only if the properties of the constituent atoms (e.g., electronic structure) are affected differently by pressure, such as the $4f$ delocalization in rare earth MGs and, in this case, an enhanced overlap of Ca $3d$ with Al $3p$ orbitals, that the electron topology is reorganized and the volume ratio is modified. This is a guiding principle to explain structural transformation phenomena in metallic glasses. The pressure-induced aggregation of Al atoms in the matrix of a Ca-rich metallic glass shows a resemblance to the recently reported nanoglass [21]. This may imply that pressure can be exploited to create nanostructures. This nanoglass has been shown to possess different electronic and physical properties from the bulk. The theoretical analysis presented here has led to a different understanding of the structure and structural transformations in compressed MGs.

ACKNOWLEDGMENTS

This work was supported by the National Key Basic Research Program of China (2012CB825700), NNSF of China (Grants No. 51371157 and No. U1432105), NSF of Zhejiang Province (Grants No. LY13E010001 and No. LQ16E010003), the Fundamental Research Funds for the Central Universities, the National Science and Engineering Research Council of a Discovery grant (Canada), and the National Science Foundation of China (11474126). Computer resources at Westgrid (Canada) and National Supercomputer Center in Tianjin are gratefully acknowledged.

M.W. and H.L. contributed equally to this work.

[1] X. J. Chen *et al.*, Proc. Natl. Acad. Sci. U.S.A. **105**, 20 (2008).
[2] C. S. Yoo, H. Cynn, F. Gygi, G. Galli, V. Iota, M. Nicol, S. Carlson, D. Häusermann, and C. Mailhiot, Phys. Rev. Lett. **83**, 5527 (1999).
[3] J.-P. Rueff, C.-C. Kao, V. V. Struzhkin, J. Badro, J. Shu, R. J. Hemley, and H. K. Mao, Phys. Rev. Lett. **82**, 3284 (1999).
[4] S. K. Deb, M. Wilding, M. Somayazulu, and P. F. McMillan, Nature (London) **414**, 528 (2001).
[5] C. A. Tulk, R. Hart, D. D. Klug, C. J. Benmore, and J. Neuefeind, Phys. Rev. Lett. **97**, 115503 (2006).
[6] J. P. Itie, A. Polian, G. Calas, J. Petiau, A. Fontaine, and H. Tolentino, Phys. Rev. Lett. **63**, 398 (1989).
[7] W. A. Crichton, M. Mezouar, T. Grande, S. Stolen, and A. Grzechnik, Nature (London) **414**, 622 (2001).
[8] P. F. McMillan, M. Wilson, D. Daisenberger, and D. Machon, Nat. Mater. **4**, 680 (2005).
[9] H. W. Sheng, W. K. Luo, F. M. Alamgir, J. M. Bai, and E. Ma, Nature (London) **439**, 419 (2006).
[10] Q.-s. Zeng, Y. Ding, W. L. Mao, W. Yang, S. V. Sinogeikin, J. Shu, H.-k. Mao, and J. Z. Jiang, Phys. Rev. Lett. **104**, 105702 (2010).
[11] G. Li, Y. Y. Wang, P. K. Liaw, Y. C. Li, and R. P. Liu, Phys. Rev. Lett. **109**, 125501 (2012).
[12] H. B. Lou *et al.*, Sci. Rep. **2**, 376 (2012).
[13] Q. S. Zeng, V. V. Struzhkin, Y. Z. Fang, C. X. Gao, H. B. Luo, X. D. Wang, C. Lathe, W. L. Mao, F. M. Wu, H.-K. Mao, and J. Z. Jiang, Phys. Rev. B **82**, 054111 (2010).
[14] H. W. Sheng *et al.*, Nat. Mater. **6**, 192 (2007).
[15] Q. S. Zeng *et al.*, Proc. Natl. Acad. Sci. U.S.A. **104**, 13565 (2007).
[16] J. Hafner and S. S. Jaswal, Phys. Rev. B **38**, 7320 (1988).
[17] M. Wu, J. S. Tse, S. Y. Wang, C. Z. Wang, and J. Z. Jiang, Nat. Commun. **6**, 6493 (2015).
[18] L. B. Valdes, Proc. IRE **42**, 420 (1954).
[19] See Supplemental Material at http://link.aps.org/supplemental/10.1103/PhysRevB.94.054201 for details of the theoretical and experimental methods.
[20] H. Liu *et al.*, J. Chem. Phys. **143**, 164508 (2015).
[21] H. Gleiter, Beilstein J. Nanotechnol. **4**, 517 (2013).
[22] Q. S. Zeng *et al.*, Science **332**, 1404 (2011).
[23] H. W. Sheng, E. Ma, H. Z. Liu, and J. Wen, Appl. Phys. Lett. **88**, 171906 (2006).
[24] M. Pozzo, M. P. Desjarlais, and D. Alfe, Phys. Rev. B **84**, 054203 (2011).